Seasonal Changes in the Sediment Flux on Steep Hillslopes in a Humid Diurnal Frost Environment

Seasonal Changes in the Sediment Flux on Steep Hillslopes in a Humid Diurnal Frost Environment

Fumitoshi IMAIZUMI[a*], Osamu SUZUKI[b], Asako TOGARI-OHTA[c]

[a] Faculty of Agriculture, Shizuoka University
836 Ohya, Suruga-ku, Shizuoka-shi, Shizuoka-ken, 422-8529, Japan

[b] Disaster Prevention Research Laboratory, R & D Center of JR-East Group, East Japan Railway Company
2-479 Nisshin-cho, Kita-ku, Saitama-shi, Saitama-ken, 331-8513, Japan

[c] Technology Planning Department, East Japan Railway Company
2-2-2 Yoyogi, Shibuya-ku, Tokyo, 151-8578 Japan

[*]corresponding author. Tel: +81-54-238-4845; Fax: +81-54-238-4845

E-mail address: imaizumi@cii.shizuoka.ac.jp (F. Imaizumi)

Abstract

Mountain hillslopes are generally shaped by a combination of various types of sediment transport processes (e.g., surface erosion, soil creep, and dry ravel), which can occur simultaneously in the same area. Since sediment transport is generally affected by multiple microclimatic factors, such as heavy rainfall and changes in ground temperature, the types of predominant sediment transport processes vary by season. We conducted field observations in the southern Japanese Alps in the period from 2009 to 2013, using sediment traps and time lapse cameras, to investigate the seasonal changes in the type and flux of hillslope sediment transport on steep mountains in which both rainfall and diurnal freeze-thaw triggered sediment transport. In winter and early spring, sediment transport via diurnal freeze-thaw (soil creep and dry ravel) was highly active, whereas rainfall-induced soil creep and selective transport by overland flow were active in summer and autumn when precipitation is abundant (average sediment flux of 0.033 and 0.074 kg m^{-1} day^{-1}, respectively). Sediment flux was spatially variable and was affected by the form of the slope; sediment flux on the concave slope was higher than on the ridge-shaped slope during both freeze-thaw and rainfall periods. Sediment flux on an old landslide exceeded that in second-growth forest regardless of the slope shape. Temporal changes in the sediment flux were not completely synchronized among monitoring plots and were affected by slope shape, grain size, and episodic sediment supply events such as release of sediment from woody debris.

Keywords: surface erosion, diurnal freeze-thaw, soil creep, dry ravel, sediment flux

INTRODUCTION

Mountains hillslopes are generally shaped by a combination of various types of sediment transport processes (e.g., surface erosion, soil creep, and dry ravel), which can occur simultaneously in the same area (e.g., Roberts and Church, 1986; Benda, 1990; Imaizumi *et al*., 2015). The sediment transport is generally affected by microclimatic factors, such as rainfall and changes in ground temperature (e.g., Inbar *et al*., 1998, Boelhouwers *et al*., 2003; Harris *et al*., 2008; Ueno *et al*., 2015). Therefore, the types of predominant sediment transport processes vary by season associated with differences in microclimatic factors. The predominant sediment transport processes are also spatially variable even on the same slope because the microtopography affects the magnitude of the driving force (i.e., gravity along the slope direction) as well as the amount of water and sediment supply from the contributing area (e.g., Roering *et al*., 1999; Fukuyama *et al*., 2010). An understanding of such seasonal and spatial changes in sediment transport activity is important for designing strategies for the protection of aquatic ecosystems as well as the mitigation of sediment disasters (Sidle and Ochiai, 2006; Gomi *et al*., 2010). In addition, steep mountains are usually the important source zones of sediment in watersheds (Imaizumi and Sidle, 2007; Struck *et al.*, 2015). Hence, an understanding of the sediment transport processes on steep hillslopes in mountains is essential to elucidate sediment budgets in entire watersheds.

Sediment transport on hillslopes has been studied in various climatic conditions around the world. In tropical and subtropical regions, numerous studies have focused on rainfall-induced sediment transport such as surface erosion and landslides (Larsen and Simon, 1993; Hartanto *et al*., 2003; Sidle *et al*., 2006). Rainfall factors (e.g., rainfall intensity and total rainfall), which affect the discharge of surface flow as well as the groundwater

level, sometimes display strong positive relationships with the sediment transport rate in such areas (Larsen and Simon, 1993; Hartanto *et al*., 2003; Sidle *et al*., 2006). In contrast, periglacial processes (i.e., soil creep and dry ravel caused by freezing-thawing) are predominant in subarctic (and sub-Antarctic) regions and high-elevation areas (Matsuoka, 2001; Boelhouwers *et al.*, 2000; Harris *et al.*, 2008). The activity of diurnal freeze-thaw cycles is explained by the frequency of the freezing (and thawing) cycles, whereas the depth of freezing is significant with regard to the activity of seasonal freezing-thawing (Matsuoka, 1998; Boelhouwers *et al*., 2003; Kværnø and Øygarden, 2006; Ueno *et al.*, 2015). Such freeze-thaw studies have been mainly performed at high-latitude or alpine regions. Meanwhile, many mountain ranges with active geomorphic processes, such as the Alps, Rocky Mountains, Southern Alps (New Zealand), and Japanese Alps, are located between tropical (subtropical) and cold regions (e.g., mid-latitude and subalpine regions). In such zones, seasonal changes in the sediment transport activity is evident because of the compound effect of rainfall and freeze-thaw on the sediment transport (Descroix and Claude, 2002; Descroix and Mathys, 2003; Regüés and Gallart, 2004; Imaizumi *et al.*, 2015). Many studies in such zones focus on the effect of freeze-thaw on activities of soil erosion by overland flow (Descroix and Claude, 2002; Regüés and Gallart, 2004; McCool *et al*., 2013), under the conditions that the erosion by overland flow is the predominant sediment transport process in all seasons. However, there have been few studies on the seasonal changes in the type of the sediment transport, including surface erosion and solifluction (Boelhouwers, 1998; Imaizumi *et al.*, 2015; Luffman *et al*., 2015).

In addition to microclimatic conditions, hillslope topography is also an important factor affecting the type of sediment transport (Sidle and Ochiai, 2006, Imaizumi *et al.*, 2015). For example, the sediment transport rate caused by surface erosion is explained by

slope gradient, slope profile, and contributing area (Hewitt, 1996; Desmet *et al.*, 1999). The activity of dry ravel, the gravitational transport of surface materials by rolling, sliding, and bouncing across the surface, has a positive relationship with steep gradient (Maita, 1985; Gabet, 2003; Sidle and Ochiai, 2006; Imaizumi *et al*., 2006). Thus, the sediment transport rate on hillslopes is spatially variable due to local topography. Consequently, it is necessary to consider the topography of the hillslope together with the microclimatic conditions to explain the dominant sediment transport processes.

The aim of this study was to clarify the seasonal changes in the type and flux of sediment transport on steep hillslopes located in an area with both abundant precipitation and active diurnal freeze-thaw activities. We conducted field observations of seasonal changes in sediment flux in the southern Japanese Alps, using sediment traps and time lapse cameras. In addition to the abundant precipitation, active sediment transport associated with freezing-thawing has also been observed in this area because of its high elevation (>1000 m) (Imaizumi and Ueji, 2012; Ueno *et al.*, 2015). We investigated the types of predominant sediment transport processes by comparing the temporal changes in the sediment flux and grain size of the transported sediment against microclimatic factors. We also investigated the effects of the microtopography (i.e., slope shape, slope gradient) on the types of sediment transport processes and the sediment flux.

We focused on the sediment transport processes on the ground surface and in the subsoil, such as surface soil erosion, surficial soil creep, and dry ravel (Hewitt, 1996; Gabet, 2003; Matsuoka, 2001). We did not investigate sediment transport in deeper soil, such as deeper soil creep (<0.05 m in depth) and landslides (Young, 1960; Barr and Swanston, 1970; Sidle and Ochiai, 2006).

STUDY SITE

We conducted field observations in the Ikawa University Forest of the University of Tsukuba, central Japan (Figure 1), located in the Akaishi Mountains, which have the highest uplift rate in Japan (4 mm yr^{-1}) (Danbara, 1971). Since the area lies in the East Asia Monsoon region, annual precipitation is high (an annual average of 2800 mm from 1993 to 2002) (Imaizumi *et al*., 2010). Heavy rainfall events (daily rainfall >100 mm day^{-1}) occur during the Baiu rainfall season (rainy season due to seasonal rain front generally from the first half of June to the second half of July) and in the autumn typhoon season (late August to early October). Winter snowfall occurs from December to March, but precipitation in this period accounts for only about 15% of the total annual precipitation. The annual maximum depth of snow cover is usually less than 20 cm and most of the snow melts within a week after the snowfall. The average erosion rate in the Ikawa University Forest, as estimated from changes in the volume of deposits in the Ikawa Dam reservoir (13 km downstream of the catchment) from 1967 to 1991 divided by the contributing area of the reservoir, is 7 mm yr^{-1}. The main geologic unit is Shimanto Cretaceous strata comprised of sandstone and shale. From 27 October to 28 October 2009, we established two study sites in the Ikawa University Forest: a secondary growth forest site (site F) and an old landslide site (site L). The two study sites were selected in order to investigate difference in seasonal sediment transport characteristics between stable (site F) and unstable (site L) sites. Both sites were located on west-facing slopes, but the slope direction varied slightly among plots and was affected by the microtopography.

A significant proportion of the trees in the secondary growth forest site (site F) was harvested in the 1950s and 1960s, but negligible anthropogenic disturbances have occurred since the harvesting. Site F is now composed of diverse species of deciduous

trees (i.e., *Quercus crispula Blume*, *Acer palmatum*) and the age of the dominant trees is 30–40 years. Herbaceous annuals (e.g., *Leucosceptrum japonicum*) cover about 20% of the ground area. The ground surface is covered by gravel and litter with a small amount of fine sediment (grain size <1 mm) and decomposing organic matter. Subsoil also contains some organic matter affected by decay of roots, mixture with surface soil by soil fauna, and probably sediment transport. To determine the differences in sediment flux for different topographies, we installed three monitoring plots at site F: ridge (FR, convex slope shape along cross-sectional direction), valley (FV, concave slope shape along cross-sectional direction), and planar/straight slope plots (FS, flat slope shape along cross-sectional direction). Slope gradients, estimated from contour lines constructed from the 1-m resolution DEM (Digital Elevation Model) obtained by airbone LiDAR (Light Detection and Ranging) scanning, were similar among the three plots (38–41°), but the contributing area differed significantly among the plots, ranging from 6.5 to 1493.6 m^2. The soil depth at site F, measured using the cone penetration test, was ranging from 0.85 to 1.75 m (average 1.18 m).

The old landslide site (site L) was located approximately 1.2 km north of site F. Three monitoring plots, LR, LV, and LS (located on the ridge, valley, and planar/straight slopes, respectively) were distributed on the landslide scar. There are no records of the exact time of occurrence of the landslide, but it can be identified by analysis of aerial photographs taken in 1963 and thus existed at least 50 years ago. Reoccurrence of failure at the southern end of the original landslide was identified in aerial photographs taken in 1984. All monitoring plots in the site L were located outside of this reoccurrence area. The landslide scar is now covered by a crown of trees located just outside the landslide ridge and those surviving at some locations in the landslide scar. However, recovery of

vegetation in the landslide scar is limited to herbaceous annuals (e.g., *Leucosceptrum japonicum*), covering less than 10% of the ground surface mainly composed of gravel and litter. Almost no recovery of young trees are found on the landslide scar. The subsoil is mainly composed of gravel with a small amount of organic matter; the proportion of organic matter at the ground surface and in the subsoil at site L is less than that at site F. The slope gradient at site L, ranging from 41 to 43°, is similar to or slightly steeper than that at site F (Table 1). The elevation at site L (about 1270 m a.s.l.) is slightly higher than that at site F (about 1110 m a.s.l.). Similar to site F, the contributing area at site L differs significantly among plots, ranging from 6.9 to 1823.0 m^2. Some woody debris with length of several meters, which captures sediment from upper slopes, was found on the slope above plot LS.

The ground surface material (depth <0.05 m) in the observation plots was sampled for grain size analysis by sieving (Figure 2). The ground surface material in LV was too coarse for analysis using sieves, and the grain size distribution in this plot was measured using the line grid method (Kato *et al.*, 1996) with a grid size of 0.3 m. The grain size of the ground surface material in the Ikawa University Forest can be characterized as containing a large fraction of coarse sediment; gravel and cobbles occupy >70% of all material in all plots (Figure 2). The differences in the grain size distribution among the monitoring plots were not clearly defined except for plot LV whose ground surface lacked fine particles (<10^{-2} m).

METHODOLOGY

Meteorological conditions

The air temperature at 1.5 m above the ground surface was measured using temperature and relative humidity data loggers (Onset Computer Co., HOBO U23 Pro v2)

at plots LS and FS. The ground surface temperature was measured using temperature loggers (Onset Computer Co., TidbiT TBI32–20+50) at all of the monitoring plots. The ground temperature sensors were covered by sediment (depth <1 cm) from the monitoring sites so that the albedo of the sensors was similar to that of the ground surface at the monitoring sites. Monitoring of the ground surface temperature at plot LR was started on 28 October 2009, and monitoring of ground surface temperature at other plots and monitoring of air temperature at all plots were started between 14 and 21 April 2010. Logging intervals of air and ground temperatures were set at 10 min.

Precipitation was measured using a tipping bucket rain gauge (tip at 0.5 mm) located between sites L and F. The rain gauge was not equipped with a heater because of the lack of an electric power supply at the monitoring site. Therefore, the timing of precipitation that occurred as snow contained errors (estimated maximum error 10 days).

Sediment transport

Sediment traps were installed to record the rates of sediment transport by ground surface and near-surface processes. Vertical wire meshes (1.75 m wide) were secured on the hillslope using steel bars (Figure 3a). Synthetic sheets were placed on the upslope side of the wire mesh and adjacent ground surface to facilitate capture of finer sediments (e.g., sand and silt), as well as to distinguish between residual soil and sediment transported from the upper slopes. Sediment stored in the traps was collected 10 times between 27 October 2009 and 3 December 2013 (Table 2). Sampling intervals varied from 41 to 364 days, but generally we attempted to capture the major periods of potential seasonal differences (i.e., the Baiu and typhoon seasons, and extreme periods of freezing and thawing) that would affect the type of sediment transport. Periods 1 and 8 mainly focused on the freeze-thaw

season, which generally starts at middle of December and ends beginning of April (Table 3a), and did not include Baiu rainfall and typhoon seasons. Periods 2, 3, 5, 6, 9, and 10 mainly focused on the Baiu and typhoon seasons (rainfall seasons; Table 2); almost no freeze-thaw cycles (i.e., the number of cycles that the ground surface temperature rose above and fell below 0ºC) were recorded in these periods (Table 2). Observation using the sediment traps was not conducted in period 7 (from 7 December 2011 to 5 December 2012) because of our schedule conflicts. Period 4, also prolonged our schedule conflicts, includes both freeze-thaw and Baiu rainfall seasons; thus, we avoided discussion on specific sediment transport processes using data in this period.

Sediments larger than 30 mm stored by the traps were separated into three classes (30–50, 50–100, and >100 mm) by measuring their diameter with a ruler. Each sediment class was weighed in the field using a spring balance. Sediments <30 mm in diameter were taken to the laboratory. After drying in a drying oven at a temperature of 105ºC for about eight hours, large organic materials (>4 mm) were removed by hand. Then, the grain-size distribution was analyzed using sieves with mesh sizes of 0.25., 0.5., 1, 2, 4, 8, and 16 mm. Since the side of the sediment traps was not closed, a portion of the sediment entrained by surface erosion washed away through the side of the traps by surface runoff. To examine the proportion of the sediment washed away, we also installed small sediment traps 1 m in width that had both sides closed (closed-type traps) at LS and US on 5 December 2012. Some of the sediment captured by the sediment traps was also transported as rock fall and dry granular flows (a mixture of sediment and interstitial air). In this study, we designated the movement of individual particles as dry ravel because of the difficulty in distinguishing the sediment transport type based on observations using the sediment traps. Since the synthetic sheets were fixed on the ground surface and captured sediment arriving onto the

sheets, they did not measure soil creep in the subsoil (>0.05 m in depth).

Photographs of the ground surface at FS were taken with a digital camera (Nikon COOLPIX4500) at intervals of 24 hours. The timing of sediment transport in a 3 x 3 m area was investigated by comparing the location of the sediments that were clearly identifiable (grain size >1 cm) in two successive photographs. Sediment transport identified in the photographs was classified into two primary types: creep and individual transport. Creep is transportation of grouped sediment such as needle ice creep, seasonal frost creep, and other types of soil creep. Creep often occurred throughout the analysis area, but also occurred in only a limited part of the study area on other days. Previous field studies have shown that the velocity of creep is sometimes very slow (<1 mm day^{-1}) (Young, 1978; Matsubayashi and Tamura, 2005). Because of limitations in the resolution of camera images (about 1 mm/pixel in the study area), we were only able to identify creep with velocity >1–2 mm day^{-1}. Slow creep (<1 mm day^{-1}) was not investigated in this study. Individual transport is movement of a single or several particles with different velocities than the surrounding sediment particles. Dry ravels and rock falls are mainly classified as individual transport. Individual transport was identified on numerous creep days in the study area. Since individual transport is often triggered by soil creep (Gabet, 2003; Imaizumi *et al.*, 2015), the separation of “creep days” from “days with creep and individual transport” is meaningless. Thus, we included “days with creep and individual transport” as “creep days” in this study. We also investigated snow cover periods from photographs; we designated snow cover days as days when more than 30% of the ground surface in the photographs was covered by snow. The sediment transport (both creep and individual transport) on such days could not be determined from the photographs because of the snow cover. Since observation using the digital camera was occasionally interrupted by mechanical problems,

photographs of the ground surface were also taken by a second camera (Brino, GardenWatchCam) at 24-hour intervals as a back-up.

RESULTS

Temperature and precipitation

The air temperature at site L was slightly lower than at site F because of the higher elevation of the former, resulting in a slightly lower ground surface temperature at site L (Figure 4a, Table 3). The ground surface temperature rose above and fell below 0ºC, which is regarded as the freezing temperature of soil water (e.g., Matsuoka, 2001; Vieira *et al.*, 2003), frequently from December to March at all of the monitoring plots (Figure 4a, Table 3a). Minimum ground surface temperature differed amongst year and plots, ranging from -2.6 to -9.5ºC (Table 3b). Diurnal changes in the ground surface temperature were more marked in winter and spring than in summer; e.g., diurnal changes in the ground surface temperature at FS in March and July were 5.2 and 3.3ºC, respectively. The total frequency of the freeze-thaw cycles in the study period ranged from 194 to 293 (average 245, Table 4). The slope direction (west-northwest) of FS partly limits the amount of direct sunshine reaching the ground surface, resulting in a lower ground surface temperature in the daytime in winter compared to the other monitoring plots (Table 4, Figure 4a). Freezing periods at FS sometimes continued for two or three days because of the low maximum daily temperature (<0ºC); thus, the frequency of freeze-thaw cycle was lower than the other five monitoring plots in which duration of one freeze-thaw cycle is generally within one day (Table 4). The ground surface temperature was almost constant at 0ºC when the ground was covered by snow.

Precipitation at the observation sites was high in the Baiu rainfall season (from

early June to late July) and the typhoon season (from August to October; Figure 4b). The maximum daily precipitation during the observation period was recorded on 19 July 2011 (409.5 mm, period 4) affected by Typhoon Ma-on. The other two days on which the daily precipitation exceeded 300 mm (3 September 2011, 21 September 2011; period 5) were also affected by typhoons.

Sediment transport

The occurrence of sediment transport was identified by the observations using sediment traps in both the rainfall and freeze-thaw seasons (Figure 4c). The sediment flux, i.e., the weight of the sediment captured by the sediment traps divided by the duration of the sampling period and width of the traps, was about two-fold higher at site L than at site F. The sediment flux on the valley-shaped slopes (LV and FV) was generally higher than that on the ridge-shaped slopes (LR and FR); p-values for the difference in the sediment flux between valley- and ridge-shaped slopes in sites L and F were below 0.05 and 0.01, respectively. The average sediment fluxes among six plots at freeze-thaw seasons (periods 1 and 8) and rainfall seasons (periods 2, 3, 5, 6, 9, and 10) were 0.074 and 0.033 kg m^{-1} day^{-1}, respectively. The sediment flux at LV in the freeze-thaw seasons was clearly higher than that in the rainfall seasons (p-value = 0.01), whereas no similar trend was observed in the other traps (p-values >0.05). The temporal changes in the sediment flux differed among sites. The fraction of fine sediment (<2 mm) captured by the closed-type traps (monitoring period: periods 7 and 8) at FS and LS (1.8% and 2.4%, respectively) was similar to that measured by the open-type traps (Figure 5). In addition, fluxes of the fine sediment observed by the open-type traps (2.1×10^{-5} and 2.5×10^{-3} kg m^{-1} day^{-1} for FS and LS, respectively) were similar or larger than that by the closed-type traps (2.1×10^{-5} and 4.7 x

10^{-4} kg m^{-1} day^{-1} for FS and LS, respectively). Therefore, the loss of fine sediment from the open-type traps appeared to have had no significant effect on determining the seasonal and spatial trends in the sediment flux.

The grain size of the sediments captured by the sediment traps differed significantly among seasons (Figure 5). It was coarser in the freeze-thaw seasons than in the other seasons in all of the sediment traps.

The timing of sediment transport, investigated using time lapse cameras, differed between the rainfall and freeze-thaw seasons (Figure 6). In the freeze-thaw season (mainly from December to March), most of the sediment transport occurred on days on which the ground surface temperature was below 0ºC in the morning, but rose above 0ºC during the daytime (Figure 6b). However, sediment transport was also observed on some days on which the ground surface temperature monitored by the temperature logger did not fall below 0ºC in the morning (e.g., in the period from 10 to 14 December 2011). Sediment transport (creep and individual transport) on these days occurred over a portion of the analysis area. Active sediment transport was also monitored in every April, but no freezing-thawing or heavy rainfall were observed on sediment transport days (Figure 6c). Most of the sediment transport in other seasons was associated with heavy rainfall events (Figure 6a); creep frequently occurred on days when the maximum rainfall intensity exceeded 20 mm, and individual transport occurred on days with less rainfall.

The total frequency of sediment transport (creep plus individual transport) was highest in early spring (55% and 64% for March and April, respectively) and lowest in November (Figure 7). The type of sediment transport varied by season. Creep type sediment transport was frequent in the period with high freeze-thaw activity (December to March). In contrast, individual transport was predominant in seasons with high precipitation

(June to September).

Although the timing of sediment transport during the rainfall seasons was strongly affected by the timing of rainfall events (Figure 6a), the sediment flux in the rainfall seasons observed using the sediment traps showed no distinct relationship with total rainfall and rainfall intensities (p-values for linear regressions > 0.1; Figure 8). The sediment flux in period 5 (0.060 kg day^{-1} m^{-1}), when the total rainfall, maximum daily rainfall, and maximum hourly rainfall were at their highest among the 6 periods in the rainfall seasons, was also highest among the rainfall seasons, but there were no clear relationships between sediment flux and rainfall factors in the other periods.

DISCUSSION

Diurnal freeze-thaw

Diurnal changes in the ground surface temperature were more marked in winter and spring than in summer (Figure 4a). Because the leaves of deciduous trees at the study sites are shed in autumn, direct sunlight hitting the ground surface raises the ground surface temperature in winter and early spring. In addition, the ground surface temperature in the morning was lowered by nocturnal radiative cooling. Such vegetation conditions likely facilitated frequent freeze-thaw cycles of the ground surface temperature at the monitoring sites (Table 3a). Temporal changes in the ground surface temperature indicate that diurnal freeze-thaw cycles, which trigger needle ice creep, shallow frost creep, and dry ravel (Matsuoka, 2001; Imaizumi *et al*., 2015), are more important periglacial processes than seasonal freezing-thawing, which causes deeper frost creep (Figure 4a, Table 4). In fact, soil creep associated with diurnal freezing-thawing was frequently observed in winter and early spring (Figure 6b), resulting in high sediment flux in those periods (Figure 4c). We

were only able to monitor the timing of faster soil creep (1–2 mm day^{-1}) using time lapse cameras (Figures 6b, 7). Since the height of frost heave is low on days with less soil moisture (Meentemeyer and Zippin, 1981; Boelhouwers *et al.*, 2003; Ueno *et al.*, 2015), it is probable that the frequency of soil creep was even higher when we consider the slower creep on dry days. The importance of diurnal freeze-thaw has also been emphasized with respect to other monitoring sites on mountains in humid monsoon areas (Matsuoka, 1998; Imaizumi *et al*., 2006), whereas surface erosion during rainfall seasons is the only important sediment transport process in some warmer and lower elevation areas (Kimoto *et al*., 2002; Miyata *et al*., 2009).

Seasonal changes in the sediment transport mechanism

As noted above, the difference in the sediment flux between the freeze-thaw and rainfall seasons was most significant for plot LV among all the monitoring plots; the sediment flux in the freeze-thaw season was 5.3-fold higher than that in the rainfall seasons. (Figure 4c). Fine sediment (diameter <10^{-2} m), which is easily transported by overland flow (Edeso *et al*., 1999; Aksoy and Kavvas, 2005; Struk et al., 2015), was absent on the ground surface at LV (Figure 2), resulting in a small proportion of rainfall-induced sediment transport. The absence of fine sediment also limits diurnal freeze-thaw activity (Boelhouwers, 1998). High sediment flux in LV in winter may be affected by the long-distance transport of sediment as dry ravel and rock fall from the contribution area, in which the ground surface soil includes fine sediment, and by freezing-thawing in subsoil in plot LV which also includes fine sediment.

Monitoring by time lapse cameras detected an annual pattern that the sediment transport frequency at FS in March exceeded that in January and February, although the air

and ground surface temperatures were higher in March than in both of these months (Figure 4). Destruction of the soil structure caused by repeated freeze-thaw cycles, which increases sediment transport activities (Regüés and Gallart, 2004; Kværnø and Øygarden, 2006; McCool *et al.*, 2013), may have caused such a high sediment transport frequency in the latter half of the freeze-thaw period. The sediment transport frequency was also high in April even though diurnal freezing-thawing was less active and precipitation was low (Figures 6c, 7). Therefore, it is possible that the effects of the destruction of the soil structure in the freeze-thaw season remained in April. The direct triggers of the sediment transport in April were probably the decrease in cohesion by evaporation of soil moisture, wind, and disturbance by animals (Verity and Anderson, 1990; Gabet, 2003).

Previous studies have reported that surface erosion by overland flow is active during high-intensity rainfall events (e.g., Kimoto *et al.*, 2002; Miyata *et al*., 2009). The timing of sediment transport in the rainfall seasons in the Ikawa University Forest also coincided with the timing of rainfall events with high hourly intensity (Figure 6a). The proportion of fine sediment, which can be easily transported by overland flow (Edeso *et al*., 1999; Aksoy and Kavvas, 2005; Struk *et al.*, 2015), was higher in the rainfall seasons at all monitoring plots (Figure 5); thus, surface erosion by overland flow also occurred in the Ikawa University Forest. Individual transport of gravel, predominant in the rainfall seasons (Figure 7), may have been trigged by selective transport of the fine sediment supporting the basal part of the gravel. In contrast, the proportion of fine sediment was small in the periglacial seasons (Figure 5). Therefore, gravitational sediment transport processes (e.g., soil creep, dry ravel, and rock falls), for which mobility is not related to grain size (Matsuoka, 1998; Gabet, 2003; Dorren, 2003), were likely predominant in the freeze-thaw seasons.

Despite similar or lower freeze-thaw frequency (Table 4), the sediment flux in the

freeze-thaw season at site L generally exceeded that at site F (Figure 4c; p-values for difference between the two sites < 0.05). Grain size distribution, which affects the freeze-thaw activity (Meentemeyer and Zippin, 1981; Boelhouwers, 1998; Ogino and Matsuoka, 2007), was not significantly different at plots LS and LR than it was at site F (Figure 2); thus, differences in the sediment flux between sites F and S may not have been affected by differences in the grain size. At site L, recovery of trees was limited and the ground surface was only covered by annual grasses. Therefore, reinforcement of the soil by roots, which increases the cohesion of the soil by penetration and binding (Sidle, 1991; Imaizumi *et al*., 2008) may be a contributing factor to the higher sediment flux at site L.

The temporal changes in the sediment flux were not completely synchronized among monitoring plots (Figure 4c). Similar spatial differences in the timing of sediment transport have also been observed in other areas (Fukuyama *et al*., 2010; Imaizumi *et al*., 2015). In addition to differences in the predominant type of sediment transport process (Imaizumi *et al*., 2015; Struck *et al*., 2015), episodic and local sediment supply events may affect such differences. For example, sediment flux at LV significantly exceeded that at LS in periods 1 and 2; however, sediment flux at LS was similar to or exceeded that at LV after period 3. Release of sediment from woody debris, which protects soils from erosion (Hartanto *et al*., 2003), possibly increased the sediment flux at plot LS. Impacts of episodic sediment supply events on the sediment flux have also been observed in other areas (e.g., Kirchner *et al*., 2001; Imaizumi *et al*., 2015). Our monitoring results imply that the episodic events affect chronic sediment flux for a long duration (at least longer than one year) after the events.

Slope topography and sediment flux

With respect to the effects of slope topography on sediment flux, the sediment flux on the valley-shaped slope, which has a larger contributing area (Table 1), was higher than that on the ridge-shaped slope in the rainfall and freeze-thaw seasons at both sites L and F, implying that slope topography affects sediment flux in both seasons. Both discharge of overland flow and erosion rate have a positive relationship with source area (and slope length), although the relationship is nonlinear because of discontinuity of the overland flow and difference in types of dominant runoff processes among different spatial scale (Cerdan *et al*., 2008; Gomi *et al*., 2008; Moreno-de Las Heras *et al*., 2010). Thereby, many sediment transport models of surface erosion include parameters that can reflect the scale of the sediment source area (Renard and Freimund, 1994; Aksoy and Kavvas, 2005). On the other hand, most models of freeze-thaw only consider local freezing and transport conditions (e.g., freezing depth, soil moisture, and slope gradient), and do not take into account the contribution area (Higashi and Corte, 1971; Matsuoka, 1998). Our monitoring results suggest that topographic factors in the sediment source area (e.g., size of contributing area) should be considered when estimating the sediment flux caused by both freeze-thaw and rainfall-related processes. Such topographic factors in the source area may affect sediment transport with long travel distances (i.e., dry ravel and rock fall) rather than slow sediment transport (i.e., soil creep), which have been successfully explained by local freezing and transport conditions (Higashi and Corte, 1971; Matsuoka, 1998). Slope gradient at monitoring plots was similar or steeper than the angle of repose for the sediment in the Ikawa University Forest (37.5°) (Imaizumi and Ueji, 2012). Such steep topography probably affected the predominance of sediment transport processes with long travel distances.

Since models for the velocity of near-surface solifluction are functions of slope

gradient (Higashi and Corte, 1971; Matsuoka, 1998; Matsuoka, 2001), slope gradient may also affect differences in winter sediment flux amongst sites and regions. In fact, winter sediment flux at a steep Kumanodaira landslide scar (average slope gradient 45°) located in central Japan was similar to or higher than at site L (0.06–0.79 kg m^{-1} day^{-1}, average 0.33 kg m^{-1} day^{-1}) (Imaizumi *et al.*, 2015). In more gentler badland topography in France (average slope gradient 31°) and cropland in USA (slope gradient 9–12°), freeze-thaw contributes sediment transport by destroying soil structure and promoting surface wash in subsequent seasons, rather than by transporting directly as solifluction in winter (Descroix and Claude, 2002; Descroix and Mathys, 2003; McCool *et al.*, 2013).

SUMMARY AND CONCLUSION

Seasonal changes in the sediment flux on steep hillslopes were investigated on a landslide scar and secondary growth forest in a humid diurnal frost enviroment using field observations of sediment transport and microclimate. Our observations revealed that both sediment flux and the dominant sediment transport processes differ by season. In winter and early spring, sediment transport by diurnal freeze (soil creep and dry ravel) was highly active, whereas rainfall-induced soil creep and selective transport by surface flow were active in summer and autumn when precipitation is abundant. Sediment flux was spatially variable and affected by slope shape; sediment flux on the valley-shaped slope was higher than that on the ridge-shaped slope in both freeze-thaw and rainfall periods. The sediment flux on the old landslide exceeded that in the second-growth forest regardless of the slope shape. The temporal changes in the sediment flux were not completely synchronized among monitoring plots and were affected by local hydrogeomorphic conditions (e.g., slope shape and grain size) as well as episodic sediment supply events such as release of

sediment from woody debris.

Sediment fluxes exhibit both spatial and temporal variability. An understanding of the dominant types of sediment transport processes as well as the local hydrogeomorphic conditions is required to explain such spatial and temporal variability. Previous studies in humid monsoon areas have focused on rainfall-induced sediment transport processes; thus, further studies on the influence of microtopography (contributing area and slope shape) on freeze-thaw are especially important to fully elucidate sediment transport processes on mountains in humid monsoon areas. Our study emphasizes the importance of studies on multiple types of sediment transport processes to understand sediment transport systems on steep hillslopes in mid-latitude mountain areas.

Acknowledgement

This work was supported by JSPS KAKENHI Grant Numbers 26292077 and 26282076. We are grateful to Dr. Ryoko Nishii for assistance with fieldwork and for providing helpful comments. The monitoring site and some of the rainfall data used in this study were provided by the Ikawa University Forest, University of Tsukuba. We thank the technical staff of the Ikawa University Forest, Toru Endo, Akira Takinami, Yoshikazu Endo, and Yusuke Ueji who supported our fieldwork.

References

Aksoy H, Kavvas ML. 2005. A review of hillslope and watershed scale erosion and sediment transport models. *Catena* **64** 247–271. DOI:10.1016/j.catena.2005.08.008

Barr DJ, Swanston DN. 1970. Measurement of creep in a shallow, slide-prone till soil,

American Journal of Science **269**: 467–480. DOI: 10.2475/ajs.269.5.467

Benda L. 1990. The influence of debris flows on channels and valley floors in the Oregon Coast Range, U.S.A. *Earth Surface Processes and Landforms* **15**: 457–466. DOI: 10.1002/esp.3290150508

Boelhouwers J. 1998. Environmental controls on soil frost activity in the Western Cape Mountains, South Africa, *Earth Surface Processes and Landforms* **23**: 211–221.

Boelhouwers J, Holness S, Sumner P. 2000. Geomorphological characteristics of small debris flows on Junir's Kop, Marion Island, maritime sub–Antarctic. *Earth Surface Processes and Landforms* **25**: 341–352. DOI: 10.1002/(SICI)1096-9837(200004)25:4<341::AID-ESP58>3.0.CO;2-D

Boelhouwers J, Holness S, Summer P. 2003. The maritime subantarctic: a distinct periglacial environment. *Geomorphology* **52**: 39–55. DOI: 10.1016/S0169-555X(02)00247-7

Cerdan O, Le Bissonnais Y, Govers G, Lecomte V, van Oost K, Couturier A, King C, Dubreuil N. 2004. Scale effect on runoff from experimental plots to catchments in agricultural areas in Normandy. *Journal of Hydrology* **299**: 4–14.

Danbara T. 1971. Synthetic vertical movements in Japan during the recent 70 years. *Journal of the Geodetic Society of Japan* **17**: 100–108 (in Japanese with English abstract).

Desmet PJJ, Poesen J, Govers G, Vandaele K. 1999. Importance of slope gradient and contributing area for optimal prediction of the initiation and trajectory of ephemeral gullies. *Catena* **37**: 377–392. DOI: 10.1016/S0341-8162(99)00027-2

Descroix L, Claude J. 2002. Spatial and temporal factors of erosion by water of black marls in the badlands of the French southern Alps. *Hydrological Sciences Journal* **47**,

227–242.

Descroix L, Mathys, N. 2003. Processes, spatio-temporal factors and measurements of current erosion in the French Southern Alps: a review. *Earth Surface Processes and Landforms* **28**: 993–1011. DOI: 10.1002/esp.514

Dorren LKA. 2003. A review of rockfall mechanics and modelling approaches. *Progress in Physical Geography* **27**: 69–87.

Edeso JM, Merino A, González MJ, Marauri P. 1999. Soil erosion under different harvesting managements in steep forestlands from northern Spain. *Land Degradation & Development* **10**: 79–88.

Fukuyama T, Onda Y, Gomi T, Yamamoto K, Kondo N, Miyata S, Kosugi K, Mizugaki S, Tsubonuma N. 2010. Quantifying the impact of forest management practice on the runoff of the surface-derived suspended sediment using fallout radionuclides. *Hydrological Processes* **24**: 596–607. DOI: 10.1002/hyp.7554

Gabet EJ. 2003. Sediment transport by dry ravel. *Journal of Geophysical Research* **108(B1)**: 2049. DOI: 10.1029/2001JB001686

Gomi T, Kobayashi S, Negishi JN, Imaizumi F. 2010. Short-term responses of macroinvertebrate drift following experimental sediment flushing in a Japanese headwater channel. *Landscape and Ecological Engineering* **6**: 257–270.

Gomi T, Sidle RC, Miyata S, Kosugi K, Onda Y. 2008. Dynamic runoff connectivity of overland flow on steep forested hillslopes: scale effects and runoff transfer. *Water Resources Research* **44**: W08411. DOI:10.1029/2007WR005894

Harris C, Kern-Luetschg M, Murton J, Font M, Davies M, Smith F. 2008. Solifluction processes on permafrost and non-permafrost slopes: results of a large-scale laboratory simulation. *Permafrost and Periglacial Processes* **19**: 359–378. DOI:

10.1002/ppp.630

Hartanto H, Prabhu R, Widayat ASE, Asdak C. 2003. Factors affecting runoff and soil erosion: Plot-level soil loss monitoring for assessing sustainability of forest management. *Forest Ecology and Management* **180(1-3)**: 361–374.

Hewitt AE. 1996. Estimating surface erosion using ^{137}Cs at a semi‐arid site in Central Otago, New Zealand. *Journal of the Royal Society of New Zealand* **26**: 107–118.

Higashi A, AE Corte. 1971. Solifluction: a model experiment. *Science* **171**: 480–482, DOI: 10.1126/science.171.3970.480

Imaizumi F, Sidle RC. 2007. Linkage of sediment supply and transport processes in Miyagawa Dam catchment, Japan. *Journal of Geophysical Research* **112**: F03012, DOI: 10.1029/2006JF000495

Imaizumi F, Sidle RC, Kamei R. 2008. c*Earth Surface Processes and Landforms* **33**: 827–840. Doi, 10.1002/esp.1574

Imaizumi F, Hattanji T, Hayakawa YS. 2010. Channel initiation by surface and subsurface flows in a steep catchment of the Akaishi Mountains, Japan. *Geomorphology* **115**: 32–42. DOI: 10.1016/j.geomorph.2009.09.026

Imaizumi F, Sidle RC, Tsuchiya S, Ohsaka O. 2006. Hydrogeomorphic processes in a steep debris flow initiation zone. *Geophysical Research Letters* **33**: L10404. DOI: 10.1029/2006GL026250

Imaizumi F, Sidle RC, Togari-Ohta A, Shimamura M. 2015. Temporal and spatial variation of infilling processes in a landslide scar in a steep mountainous region, Japan. *Earth Surface Processes and Landforms* **40**: 642–653.

Imaizumi F, Ueji Y. 2012. Soil movement in artificial forests located in steep mountain area and its countermeasures using thinned woods. *Shinrin-Gakkaishi* **94(1)**: 24–30 (in

Japanese with English Abstract).

Inbar M, Tamir M, Wittenberg L. 1998. Runoff and erosion processes after a forest fire in Mount Carmel, a Mediterranean area. *Geomorphology* **24**: 17–33. DOI:10.1016/S0169-555X(97)00098-6

Kato S, Inoue K, Shimazu H. 1996. Re-examination of the analysis of grain size distributions of the coarse river-bed material by the line-grid method. *Humans and Nature* **7**: 33-41 (in Japanese with English Abstract).

Kirchner JW, Finkel RC, Riebe CS, Granger DE, Clayton JL, King JG, and Megahan WF. 2001. Mountain erosion over 10 yr, 10 k.y., and 10 m.y. time scales. *Geology* **29**: 591 – 594.

Kimoto A, Uchida T, Mizuyama T, Changhua L. 2002. Influences of human activities on sediment discharge from devastated weathered granite hills of southern China: effects of 4-year elimination of human activities. *Catena* **48**: 217– 233.

Kværnø SH, Øygarden L. 2006. The influence of freeze–thaw cycles and soil moisture on aggregate stability of three soils in Norway. *Catena* **67**: 175 – 182. DOI:10.1016/j.catena.2006.03.011

Larsen MC, Simon A. 1993. A rainfall intensity-duration threshold for landslides in a humid-tropical environment, Puerto Rico. *Geografiska Annaler Series A*, **75A**: 13 – 23.

Luffman IE, Nandi A, Spiegel T. 2015. Gully morphology, hillslope erosion, and precipitation characteristics in the Appalachian Valley and Ridge province, Southeastern USA. *Catena* **133**, 221-232. DOI:10.1016/j.catena.2015.05.015

Maita H. 1985. The movement and deposition of debris and the vegetation invasion on the landslide scars in the upper basin of the Oi River. *Journal of the Japan society of Erosion Control Engineering* **38(4)**: 16–24 (in Japanese with English abstract).

Matsubayashi T, Tamura T. 2005. Mode and Rate of Soil Creep by Soil Horizons: Device of a monitoring method and its application to forest covered hillslopes in humid temperate climate. *Journal of Geography* **114**: 751–766 (in Japanese with English abstract).

Matsuoka N. 1998. Modelling frost creep rates in an alpine environment. *Permafrost and Periglacial Processes* **9**: 397–409, DOI: 10.1002/(SICI)1099-1530(199810/12)9:43.0.CO;2-Q

Matsuoka N. 2001. Solifluction rates, processes and landforms: a global review. *Earth-Science Review* **55**: 107–134. DOI: 10.1016/S0012-8252(01)00057-5

McCool DK, Dun S, Wu JQ, Elliot WJ, Brooks ES. 2013. Seasonal change of WEPP erodibility parameters for two fallow plots on a palouse silt loam. *Transactions of the American Society of Agricultural and Biological Engineers* **56**: 711–718.

Meentemeyer V, Zippin J. 1981. Soil moisture and texture controls of selected parameters of needle ice growth. *Earth Surface Processes and Landforms* **6**: 113–125. DOI: 10.1002/esp.3290060205

Miyata S, Kosugi K, Gomi T, Mizuyama T. 2009. Effects of forest floor coverage on overland flow and soil erosion on hillslopes in Japanese cypress plantation forests. *Water Resources Research* **45**: W06402. DOI:10.1029/2008WR007270.

Moreno-de las Heras M, Nicolau JM, Merino-Martín L, Wilcox BP. 2010. Plot-scale effects on runoff and erosion along a slope degradation gradient. *Water Resources Research* **46**: W04503. DOI:10.1029/2009WR007875

Ogino Y, Matsuoka M. 2007. Involutions resulting from annual freeze–thaw cycles: a laboratory simulation based on observations in northeastern Japan. *Permafrost and Periglacial Processes* **18**: 323–335. DOI: 10.1002/ppp.597

Regüés D, Gallart F. 2004. Seasonal patterns of runoff and erosion responses to simulated

rainfall in a badland area in Mediterranean mountain conditions (Vallcebre, Southeastern Pyrenees). *Earth Surface Processes and Landforms* **29**: 755–767.

Renard KG, Freimund JR. 1994. Using monthly precipitation data to estimate the R factor in the revised USLE. *Journal of Hydrology* **157**: 287–306.

Roering JJ, Kirchner JW, Dietrich WE. 1999. Evidence for nonlinear, diffusive sediment transport on hillslopes and implications for landscape morphology. *Water Resources Research* **35**: 853–870.

Sidle RC. 1991. A conceptual model of changes in root cohesion in response to vegetation management. *Journal of Environmental Quality* **20**: 43–52.

Sidle RC, Ochiai H. 2006. Landslides: Processes, Prediction, and Land Use. *American Geophysical Union Water Resources Monograph* **18**: American Geophysical Union, Washington, DC.

Sidle RC, Ziegler AD, Negishi JN, Nik AR, Siew R, Turkelboom F. 2006. Erosion processes in steep terrain—Truths, myths, and uncertainties related to forest management in Southeast Asia. *Forest Ecology and Management* **224**: 199–225.

Struck M, Andermann C, Hovius N, Korup O, Turowski JM, Bista R, Pandit HP, Dahal RK. 2015. Monsoonal hillslope processes determine grain size-specific suspended sediment fluxes in a trans-Himalayan river. *Geophysical Research Letters* **42**: 2302–2308. DOI: 10.1002/2015GL063360

Roberts RG, Church M. 1986. The sediment budget in severely disturbed watersheds, Queen Charlotte Ranges, British Columbia. *Canadian Journal of Forest Research* **16(5)**: 1092–1106. DOI: 10.1139/x86-189

Ueno K, Kurobe K, Imaizumi F, Nishii R. 2015. Effects of deforestation and weather on diurnal frost heave processes on the steep mountain slopes in south central Japan.

Earth Surface Processes and Landforms **40**: 2013–2025. DOI: 10.1002/esp.3776

Verity GE, Anderson DW. 1990. Soil eroson effects on soil quality and yield. *Canadian Journal of Soil Science* **70**: 471–484. DOI: 10.4141/cjss90-046

Vieira GT, Mora C, Ramos M. 2003. Ground temperature regimes and geomorphological implications in a Mediterranean mountain (Serra da Estrela, Portugal). *Geomorphology* **52:** 57–72. DOI: 10.1016/S0169-555X(02)00248-9

Young A. 1960. Soil movement by denudational processes on slope. *Nature* **4745**: 120–122. DOI:10.1038/188120b0

Young A. 1978. A 12-year record of soil movement on a slope. *Zeitschrift für Geomorphologie, supplement* **29**: 104–110.

Table 1. Topography around monitoring plots

Plot name	Cross-sectional topography	Slope gradient[a] (degree)	Contributing area (m^2)
FR	ridge	38	6.5
FV	valley	41	1493.6
FS	straight	38	45.6
LR	ridge	43	6.9
LV	valley	41	1823.0 (241.2)[b]
LS	straight	43	21.9
average		41	566

a slope gradient measured 10 m upslope from sediment traps
b area located on an old landslide scar

Table 2. Sampling schedule for sediment traps. Number of freeze-thaw cycles, indicating the number of cycles that the ground surface temperature rose above and fell below 0ºC, is average of six monitoring plots.

Period	Beginning	End	Number of days	Number of freeze-thaw cycles	Important climate factors
1	27–28 Oct. 2009	7–8 Jun. 2010	222–224	48	Freezing-thawing
2	7–8 Jun. 2010	14–15 Sep. 2010	99–100	0	Rain
3	14–15 Sep. 2010	9–10 Dec. 2010	85–87	0	Rain
4	9–10 Dec. 2010	10 Aug. 2011	243–244	59	Freezing-thawing and rain
5	10 Aug. 2011	26–27 Oct. 2011	77–78	0	Rain
6	26–27 Oct. 2011	7–8 Dec. 2011	41–42	0	Rain
7	7–8 Dec. 2011	5 Dec. 2012	363–364	74	–
8	5 Dec. 2012	18 Apr.2013	134	64	Freezing-thawing
9	18 Apr. 18 2013	26 Sep. 2013	161	0	Rain
10	26 Sep. 2013	3 Dec. 2013	68	4	Rain

Table 3. Freeze-thaw periods and minimum ground surface temperature in each winter.

(a) Freeze-thaw periods

Plot name	2009–2010	2010–2011	2011–2012	2012–2013
FR	Dec. 18–Mar. 29	Nov. 30–Apr. 5	Dec. 10–Apr. 8	Dec. 7–Apr. 13
FV	Dec. 17–Mar. 30	Dec. 10–Apr. 5	Dec. 10–Apr. 8	Dec. 7–Apr. 14
FS	Dec. 17–Mar. 30	Dec. 25–Apr. 1	Dec. 17–Mar. 30	Dec. 7–Mar. 13
LR	Dec. 17–Mar. 30	Dec. 10–Apr. 5	Dec. 10–Apr. 8	Dec. 7–Apr. 13
LV	Dec. 1–Mar. 30	Jan. 7–Apr. 5	Dec. 17–Apr. 8	Dec. 11–Apr. 14
LS	Dec. 17–Mar. 30	Dec. 17–Apr. 5	Dec. 10– Mar. 29	Dec. 7–Mar. 7

(b) Minimum ground surface temperature

Plot name	Minimum ground surface temperature (ºC)			
	2009–2010	2010–2011	2011–2012	2012–2013
FR	-2.9	-6.2	-5.2	-4.8
FV	-3.4	-9.5	-6.2	-6.7
FS	-2.8	-5.5	-4.5	-3.2
LR	-3.4	-6.6	-5.0	-4.0
LV	-2.6	-3.1	-3.8	-3.8
LS	-3.4	-6.9	-4.9	-3.3

Table 4. Comparison of air and ground surface temperatures among monitoring plots. Average temperatures were calculated using data from 1 May 2010 to 30 April 2013. The frequency of freeze-thaw cycles was calculated for the entire monitoring period (21 October 2010 to 3 December 2013).

Plot name	Average air temperature[a] (ºC)	Average ground surface temperature (ºC)	Temperature in winter (ºC)		Frequency of freeze-thaw cycles at ground surface
			Average daily maximum	Average daily minimum	
FR	–	10.3	9.8	-0.6	279
FV	–	10.1	10.4	-1.4	293
FS	9.5	9.3	2.3	-0.5	194
LR	–	9.0	5.0	-0.7	261
LV	–	9.6	6.5	0.2	201
LS	8.6	8.9	4.5	-0.7	244

a air temperature was just monitored at plots FS and LS.

Figure Captions

Figure 1. Topographic map showing observation sites in the Ikawa University Forest. (a) Location of the Ikawa University Forest and observation sites. (b) Topographic map of site L. Shaded area indicates the old landslide scar. (c) Topographic map of site F.

Figure 2. Grain size distribution of soil surface material.

Figure 3. Illustration of sediment traps. (a) Open-type traps. (2) Closed-type traps.

Figure 4. Changes in the daily maximum (black line) and minimum (gray line) temperatures, daily precipitation, and sediment flux observed using sediment traps at the observation plots. (a) Air and ground surface temperatures. (b) Daily precipitation at the observation site. (c) Sediment flux. “Rainfall seasons” are periods including Baiu and/or Typhoon rainy seasons. “FT seasons” (freeze-thaw seasons) are periods when freeze-thaw cycles are frequently observed. Both freeze-thaw and rainfall seasons are included in period 4.

Figure 5. Seasonal differences in the grain size of sediment captured by sediment traps. “Rain” and “FT” at the category axis indicates sampling periods incruding rainfall seasons (Baiu and/or Typhoon seasons) and seasons with high freeze-thaw activity, respectively.

Figure 6. Timing of sediment transport (creep and individual transport) in (a) September 2011, (b) December 2011, and (c) April 2012 observed using an time lapse camera at site FS. Days on which the ground surface temperature was below 0ºC in the morning but rose

above 0ºC in the daytime are shown as freeze-thaw days. The maximum hourly precipitation on each day is also shown.

Figure 7. Monthly percentages of number of days on which creep and individual transport occurred. Percentages were calculated from the number of days on which sediment transport occurred divided by the number of days without snow cover. The percentages of snow-covered days are also shown.

Figure 8. Comparison between average sediment flux of all sediment traps and rainfall factors for each sampling period: (a) total rainfall, (b) maximum daily rainfall, (c) maximum hourly rainfall. Rainfall season, freeze-thaw season (FT season), and season including both rainy and FT seasons are plotted using different symbols.

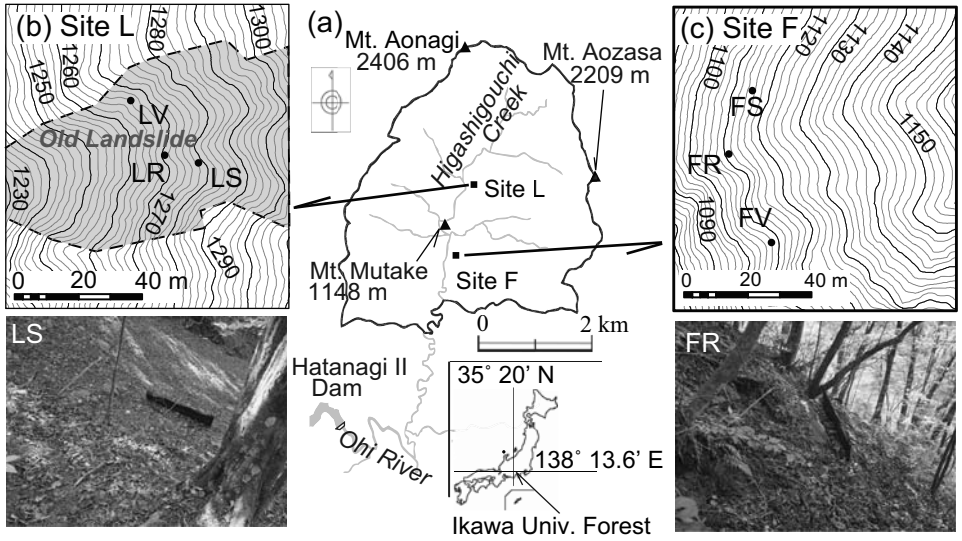
(b) Site L
1300
1280
1260
1250
LV
Old Landslide
LR
LS
1230
1270
1290
0 20 40 m
LS
(a)
Mt. Aonagi
2406 m
Mt. Aozasa
2209 m
Higashigouchi
Creek
Site L
Mt. Mutake
1148 m
Site F
0 2 km
Hatanagi II
Dam
Ohi River
35° 20' N
138° 13.6' E
Ikawa Univ. Forest
(c) Site F
1100
1120
1130
1140
1150
1090
FS
FR
FV
0 20 40 m
FR

Figure 1

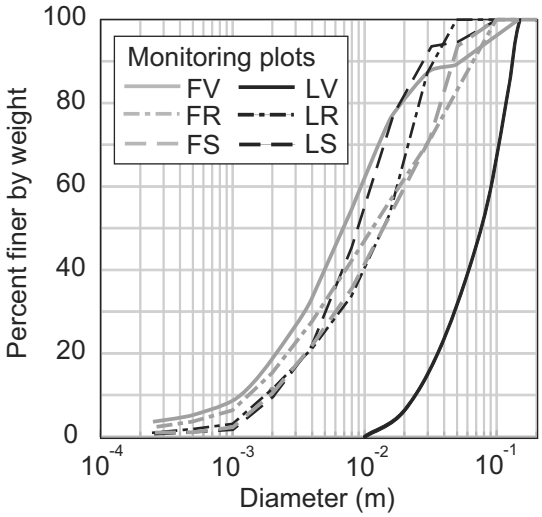
Monitoring plots
FV
LV
FR
LR
FS
LS
Percent finer by weight
100
80
60
40
20
0
10-4
10-3
10-2
10-1
Diameter (m)

Figure 2

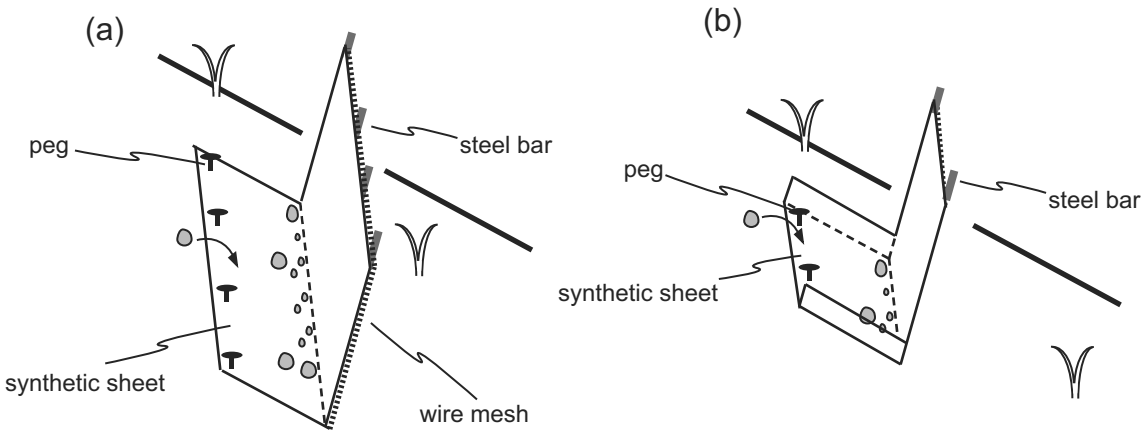
(a)
peg
steel bar
synthetic sheet
wire mesh
(b)
peg
steel bar
synthetic sheet

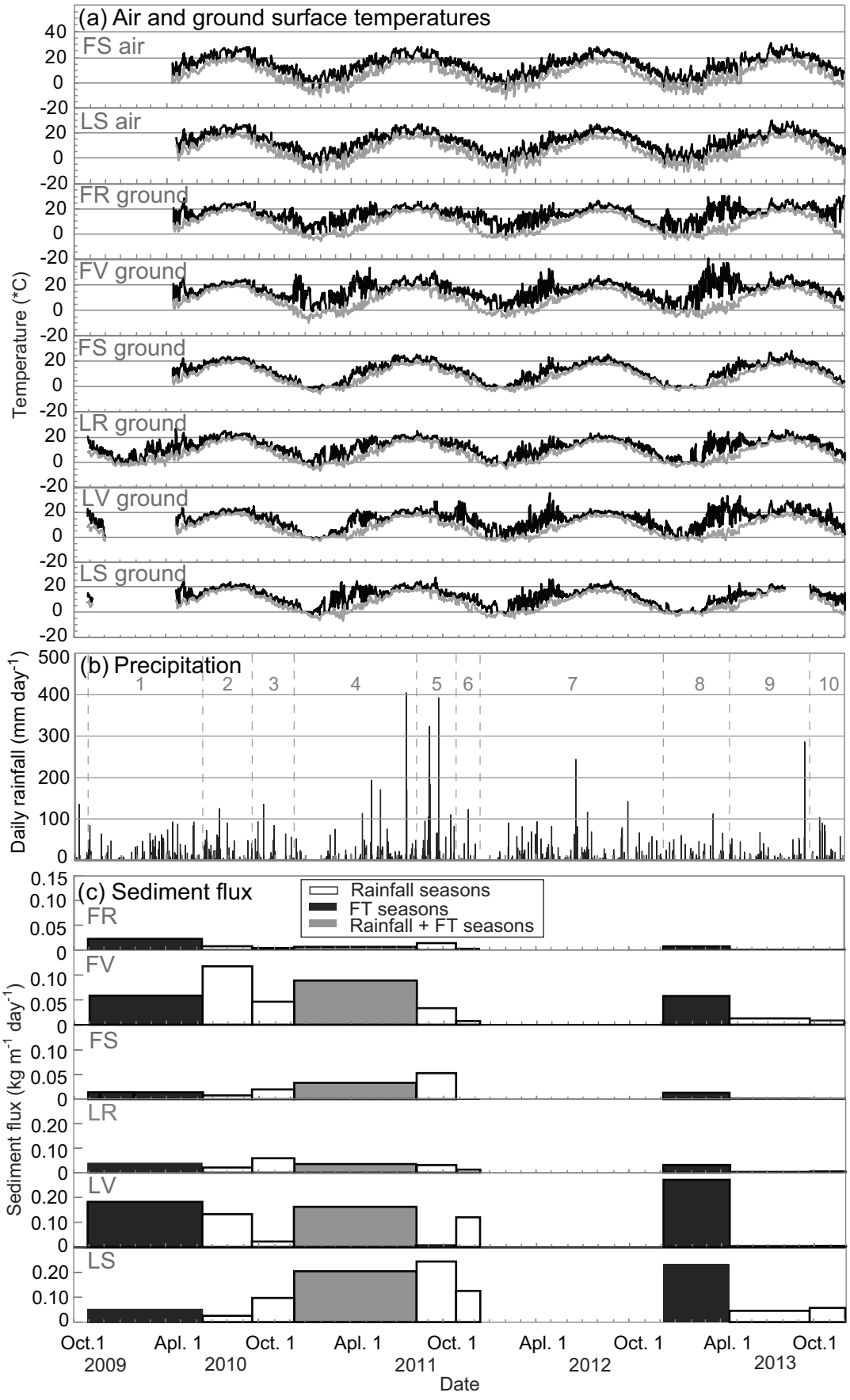
(a) Air and ground surface temperatures
FS air
LS air
FR ground
FV ground
FS ground
LR ground
LV ground
LS ground
Temperature (°C)
(b) Precipitation
Daily rainfall (mm day-1)
1
2
3
4
5
6
7
8
9
10
(c) Sediment flux
Rainfall seasons
FT seasons
Rainfall + FT seasons
FR
FV
FS
LR
LV
LS
Sediment flux (kg m-1 day-1)
Oct.1 2009
Apl. 1 2010
Oct. 1
Apl. 1
Oct. 1 2011
Apl. 1
Oct. 1 2012
Apl. 1 2013
Oct.1
Date

Figure 4

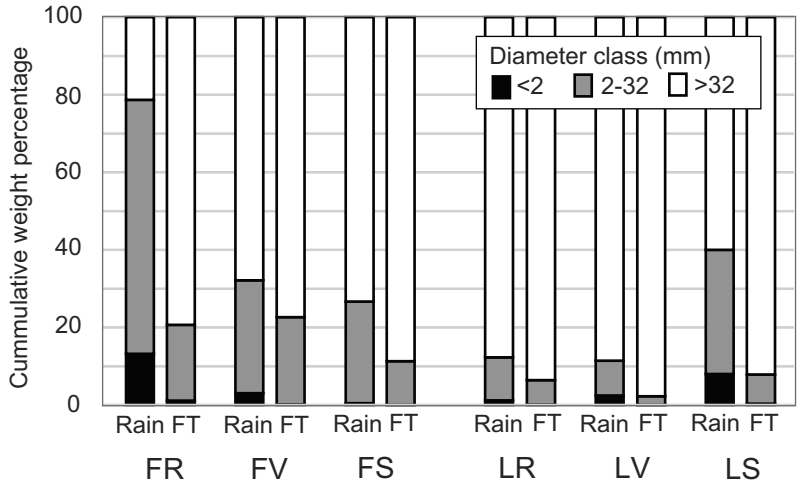
100
80
60
40
20
0
Cummulative weight percentage
Diameter class (mm)
<2
2-32
>32
Rain FT
Rain FT
Rain FT
Rain FT
Rain FT
Rain FT
FR
FV
FS
LR
LV
LS

Figure 5

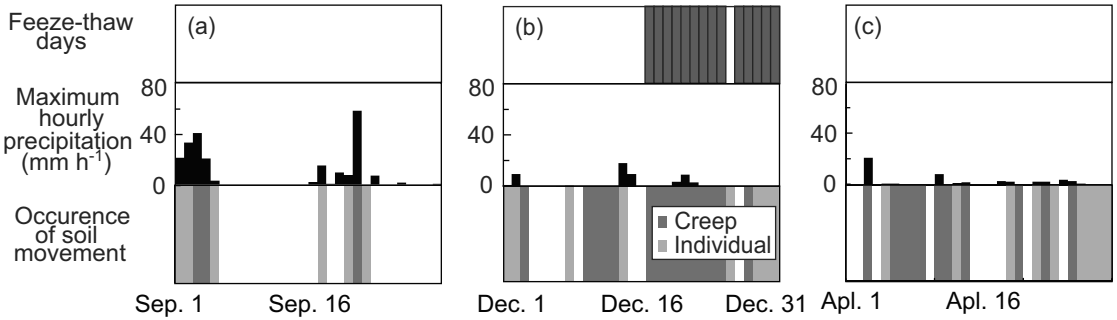
Feeze-thaw days
Maximum hourly precipitation (mm h-1)
Occurence of soil movement
(a)
(b)
(c)
80
40
0
Creep
Individual
Sep. 1
Sep. 16
Dec. 1
Dec. 16
Dec. 31
Apl. 1
Apl. 16

Figure 6

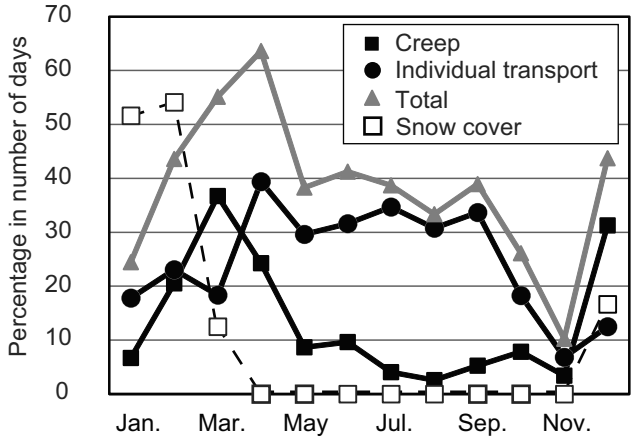
Percentage in number of days
70
60
50
40
30
20
10
0
Jan.
Mar.
May
Jul.
Sep.
Nov.
Creep
Individual transport
Total
Snow cover

Figure 7

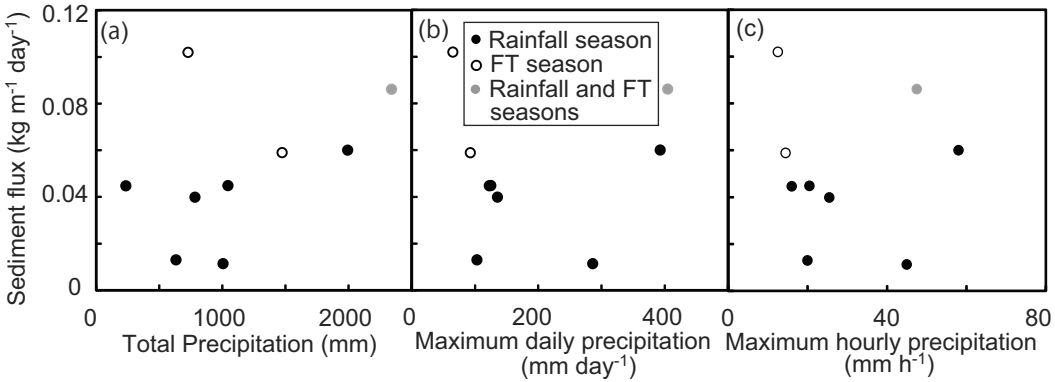
0.12
0.08
0.04
0
Sediment flux (kg m-1 day-1)
(a)
(b)
(c)
Rainfall season
FT season
Rainfall and FT seasons
0
1000
2000
Total Precipitation (mm)
0
200
400
Maximum daily precipitation (mm day-1)
0
40
80
Maximum hourly precipitation (mm h-1)

Figure 8